Naval Research Laboratory

Washington, DC 20375-5320

NRL/MR/5050--99-8381

Wave Equation Solution for Electromagnetic Field Incident on Planar Conducting Arrays

PETER LOSCHIALPO

Signature Technology Office

June 10, 1999

REPORT DOCUMENTATION PAGE

Form Approved
OMB No. 0704-0188

1. AGENCY USE ONLY (*Leave Blank*)	2. REPORT DATE	3. REPORT TYPE AND DATES COVERED
	June 10, 1999	

4. TITLE AND SUBTITLE

Wave Equation Solution for Electromagnetic Field Incident on Planar Conducting Arrays

5. FUNDING NUMBERS

6. AUTHOR(S)

Peter Loschialpo

7. PERFORMING ORGANIZATION NAME(S) AND ADDRESS(ES)

Naval Research Laboratory
Washington, DC 20375-5320

8. PERFORMING ORGANIZATION REPORT NUMBER

NRL/MR/5050--99-8381

9. SPONSORING/MONITORING AGENCY NAME(S) AND ADDRESS(ES)

Office of Naval Research
800 North Quincy Street
Arlington, VA 22217-5660

10. SPONSORING/MONITORING AGENCY REPORT NUMBER

11. SUPPLEMENTARY NOTES

12a. DISTRIBUTION/AVAILABILITY STATEMENT

Approved for public release; distribution unlimited.

12b. DISTRIBUTION CODE

13. ABSTRACT (*Maximum 200 words*)

A new wave equation solution is presented for analyzing planar periodic patch or aperture arrays having complex conductivity with an arbitrary distribution. The approach extends prior developments in photonic band-gap theory by including the conductivity mechanism. The wave equation is written in the form Schrodinger's equation. Solutions are obtained in the spectral domain for the radiated field in terms of a summation of plane waves. The method provides valuable physical insights not readily obtainable using conventional solutions for periodic arrays. Incident and radiated fields are related in a single mathematical expression. This expression shows how each radiated field mode is coupled to the others via mutual capacitive and inductive terms. The theory may be readily extended to multiple layers.

14. SUBJECT TERMS

Period planar arrays
Patch arrays
Photonic band gap
Frequency selective surfaces
Grating lobes
Antennas

15. NUMBER OF PAGES

35

16. PRICE CODE

17. SECURITY CLASSIFICATION OF REPORT	18. SECURITY CLASSIFICATION OF THIS PAGE	19. SECURITY CLASSIFICATION OF ABSTRACT	20. LIMITATION OF ABSTRACT
UNCLASSIFIED	UNCLASSIFIED	UNCLASSIFIED	UL

NSN 7540-01-280-5500

Standard Form 298 (Rev. 2-89)
Prescribed by ANSI Std 239-18
298-102

CONTENTS

I. INTRODUCTION 1

II. THEORETICAL ANALYSIS 4

III. EXPERIMENTAL VALIDATION 17

IV. CONCLUSION 22

ACKNOWLEDGMENT 23

FOOTNOTE 24

REFERENCES 25

FIGURE CAPTIONS 27

Wave Equation Solution for Electromagnetic Field Incident on Planar Conducting Arrays

Peter Loschialpo

Abstract-A new wave equation solution is presented for analyzing planar periodic patch or aperture arrays having complex conductivity with an arbitrary distribution. The approach extends prior developments in photonic band-gap theory by including the conductivity mechanism. The wave equation is written in the form Schrödinger's equation. Solutions are obtained in the spectral domain for the radiated field in terms of a summation of plane waves. The method provides valuable physical insights not readily obtainable using conventional solutions for periodic arrays. Incident and radiated fields are related in a single mathematical expression. This expression shows how each radiated field mode is coupled to the others via mutual capacitive and inductive terms. The theory may be readily extended to multiple layers.

I. INTRODUCTION

Due to their wealth of applications, two-dimensional, planar, periodic conducting arrays have received considerable attention [1-9]. They have recently been used in the design

Manuscript approved May 18, 1999.

of reflectors for lightweight spacecraft antennas[8]. The design exploits resonances in order to separate multiple, closely separated frequency bands. Accurate predictions in the presence of grating lobes is necessary for design of frequency scanning antennas [9] which are designed to efficiently couple energy into the first order grating lobe. These periodic structures may also be used as filters or polarizers. They can be applied over a wide range of the electromagnetic spectrum, from the visible to the microwave band.

The typical approach to analyzing such structures, reviewed in detail by Mittra [2] and Chan [3], uses the electric field integral equation (EFIE) relating the incident electric field to the current density in the conducting patches. Using method of moments techniques, current density is expanded as a sum of basis functions and it's coefficients are found by the solution of a matrix equation. The field radiated by the patches is subsequently calculated from the current distribution. In a similar approach, Usoff [6] and Munk [7] treated the current array as a sum of infinitesimal current filaments. These current filaments are written in a matrix equation as a function of the voltage induced on the filaments by the incident electric field. After a matrix inversion to solve for the currents, the electric field radiated by the array is calculated from the current.

Conductivity is assumed to be constant within a patch for these approaches.

A different method is described which offers potentially valuable new physical insights as well as accurate predictions. In a similar manner used to investigate photonic devices [10-11], the wave equation is written in a form analogous to Schrödinger's equation. In this case, the planar array has a periodically varying distribution of conductive patterns. The complex conductivity, or surface admittance, is expanded as a sum of exponential basis functions. Patterns may have an arbitrary shape and conductivity distribution, continuous or discrete, provided enough modes are included. This enhances design flexibility. Expressing the radiated fields as a sum of plane waves, a solution is derived in the spectral domain consistent with boundary conditions at the array and the surrounding dielectric regions. The solution relates the incident and radiated fields in a single mathematical expression, with the field modes coupled to each other by terms which may be identified as capacitive and inductive. This enables a direct examination of the strength of the interaction between field modes. It can enable a designer to more efficiently couple more energy into a particular mode of interest. The theory is extendible to multiple layers in a straightforward fashion, using the generalized scattering matrix approach.

The method of analysis is discussed in detail in Section II for a conducting planar array imbedded in a multilayered dielectric medium. A plane wave is incident to the dielectric stack at an arbitrary direction. The derived matrix equation can be solved by matrix inversion for the radiated field modes. These are then used to calculate transmission and reflection due to the dielectric stack containing the array. Validation measurements, made for array patterns on a single layer dielectric are discussed in section III.

II. THEORETICAL ANALYSIS

The analysis of the interaction of a planar periodic array of conducting shapes with an incident electromagnetic wave is in investigated through a wave equation in the form of Schrödinger's equation, used in the development of photonic band-gap theory. The complex admittance distribution leads to a matrix solution which is more complicated than that for the photonic band-gap theory. Field modes are coupled to on another by capacitive and inductive terms containing the Fourier transform coefficients of the admittance.

Begin with a thin, planar array of conducting elements. The elements lie in the plane $z = z_L$ and repeat periodically with distances d_x and d_y. The repeating elements may have any

shape and admittance distribution (see Fig. 1a). Figure 1b shows this array imbedded in a dielectric slab "m" having a uniform scalar permittivity, ε_m. Slab "m" is one of a series of M-1 slabs. Free space surrounds multilayered dielectric on both sides. Subregions of slab "m" on the left and right side of the conducting array are identified as "a" and "b", respectively.

The wave equation for the electric field in any of the dielectric regions can be written as

$$-\nabla^2\vec{E} + \nabla(\nabla \bullet \vec{E}) - i\omega\mu_o\vec{J} = \omega^2\mu_o\varepsilon\vec{E} . \qquad (1)$$

In the above equation, ω is angular frequency, μ_o is the free-space magnetic permeability, $\vec{J}$ is the current density, and $\vec{E}$ is the total vector electric field. MKS units are used. Harmonic time dependence is assumed for all fields and currents, so $\vec{E}(\vec{r},t) = \vec{E}(\vec{r})e^{-i\omega t}$. Because the conducting elements are infinitesimally thin, the z component of current density, J_3, is zero. The x and y components are given by Ohm's Law written in the form:

$$J_{1,2}(x,y,z) = \frac{E_{1,2}(x,y,z)\delta(z-z_L)}{R_S(x,y)} . \qquad (2)$$

Here $\delta(z-z_L)$ is the dirac delta function and conductivity can be identified as $\delta(z-z_L)/R_S(x,y)$. $R_S(x,y)$ is the surface impedance in the $z=z_L$ plane of the array. Note the similarity of Eq.s (1-2) with the wave equation used in photonic band-gap theory [10-11]. The periodically varying permittivity distribution is analogous to the conductivity in Eq.(2).

The electric field is next examined in detail for dielectric region "m". Subscripts "m" which apply to the field components in this region are not written, though are implicitly understood. Each vector component of the field may be written as the sum of an "incident" field, $E_i(\vec{r})$, and a "radiated" field, $\Psi_i^{a,b}(\vec{r})$, due to the array currents.

$$\mathrm{E}_i(\vec{r}) = E_i(\vec{r}) + \Psi_i^{a,b}(\vec{r}) \quad (i = 1, 2, 3) \tag{3}$$

Subscripts "a" and "b" apply to the two subregions of dielectric slab "m" on either side of the array. The subscript i = 1, 2, 3 refers to the three vector components x, y, and z.

The incident field is assumed to be a plane wave. It is written as

$$\mathrm{E}_i(\vec{r}) = (E_{i+}e^{+ik_{0,3}(z+z_L)} + E_{i-}e^{-ik_{0,3}(z-z_L)})e^{i\vec{k}_T\bullet\vec{r}}. \tag{4}$$

In Eq. (4), $\vec{k}_T$ is the component of the wave propagation vector parallel to the array. It is given by $\vec{k}_T = k_1\hat{x} + k_2\hat{y}$. The component perpendicular to the array is given by $k_{0,3} = \sqrt{\beta_m^2 - k_1^2 - k_2^2}$, where $\beta_m^2 = \varepsilon_m(\omega/c)^2$ and the free space speed of light is given by c.

The form for the radiated field components for the two subregions " a " and " b " is found by noting previous work [7]. Munk showed that the field radiated by a periodic array of linear current elements can be written as a sum of plane waves. The same is true for any current distribution which can be expressed as a sum of linear current elements. The x and y components of the radiated field are then written as:

$$\Psi_{1,2}^a(\vec{r}) = \sum_{\vec{G}} (\Psi_{\vec{G}(1,2)+}^a e^{+ik_{\vec{G},3}(z-z_L)} + \Psi_{\vec{G}(1,2)-}^a e^{-ik_{\vec{G},3}(z+z_L)}) e^{i(\vec{k}_T - \vec{G})\cdot\vec{r}} \tag{5a}$$

$$\Psi_{1,2}^b(\vec{r}) = \sum_{\vec{G}} (\Psi_{\vec{G}(1,2)+}^b e^{+ik_{\vec{G},3}(z+z_L)} + \Psi_{\vec{G}(1,2)-}^b e^{-ik_{\vec{G},3}(z-z_L)}) e^{i(\vec{k}_T - \vec{G})\cdot\vec{r}} \tag{5b}$$

$\vec{G}$ is the reciprocal lattice vector of the array. It is given by $\vec{G} = G_1\hat{x} + G_2\hat{y}$ and its components are $G_{1,2} = 2\pi n_{1,2}/d_{x,y}$, where $n_{1,2}$ = 0, ±1, ±2, ... The summation over $\vec{G}$ is taken over both components G_1 and G_2. The component of the propagation vector perpendicular to the array for these radiated modes is:

$$k_{\bar{G},3} = \sqrt{\beta_m^2 - (k_1 - G_1)^2 - (k_2 - G_2)^2} \qquad (6)$$

The incident field coefficients in Eq. (4) are related by the reflection coefficients at the $z = z_m$ boundary. This allows Eq. (4) to be written in terms of the coefficients for the negative traveling wave alone.

$$\mathrm{E}_{1,2}(\vec{r}) = (\mathrm{E}_{1,2-} S_{0(1,2)} + R_{0\otimes-} \mathrm{E}_{(2,1)-} e^{+ik_{0,3}(z+z_L-2z_m)}) e^{i\vec{k}_T \bullet \vec{r}} \qquad (7)$$

$$S_{0(1,2)}(z) \equiv e^{-ik_{0,3}(z-z_L)} + R_{0(1,2)-} e^{+ik_{0,3}(z+z_L-2z_m)} \qquad (8)$$

$R_{0(1,2)-}$ and $R_{0\otimes-}$ are the reflection coefficients (copolarization and cross polarization) at the z_m dielectric boundary for the x and y incident field components. The coefficients, $\mathrm{E}_{1,2-}$ in Eq. (7) are the input variables to the final solution.

Equations similar to (7) and (8) apply to the field in subregion "b" radiated by the array.

$$\Psi^b_{1,2}(\vec{r}) = \sum_{\bar{G}} (\Psi^b_{\bar{G}(1,2)-} S_{\bar{G}(1,2)} + R_{\bar{G}\otimes-} \Psi^b_{\bar{G}(2,1)-} e^{+ik_{\bar{G},3}(z+z_L-2z_m)}) e^{i(\vec{k}_T-\bar{G})\bullet\vec{r}} \qquad (9)$$

$$S_{\bar{G}(1,2)}(z) \equiv e^{-ik_{\bar{G},3}(z-z_L)} + R_{\bar{G}(1,2)-} e^{+ik_{\bar{G},3}(z+z_L-2z_m)} \qquad (10)$$

$R_{\bar{G}(1,2)-}$ and $R_{\bar{G}\otimes-}$ are the reflection coefficients at the $z=z_m$ boundary which relate the negative to the positive traveling modes.

Equations analogous to the radiated field in subregion "b" also apply to the field in subregion "a" radiated by the array. In this case, $R_{\bar{G}(1,2)+}$ and $R_{\bar{G}\otimes+}$ are the reflection coefficients at the $z=z_{m+1}$ boundary which relate the positive to the negative traveling radiated modes.

$$\Psi^a_{1,2}(\vec{r}) = \sum_{\bar{G}} (\Psi^a_{\bar{G}(1,2)+} C_{\bar{G}(1,2)} + R_{\bar{G}\otimes+} \Psi^a_{\bar{G}(2,1)+} e^{-ik_{\bar{G},3}(z+z_L-2z_{m+1})}) e^{i(\vec{k}_T-\bar{G})\bullet\vec{r}} \tag{11}$$

$$C_{\bar{G}(1,2)}(z) \equiv e^{+ik_{\bar{G},3}(z-z_L)} + R_{\bar{G}(1,2)+} e^{-ik_{\bar{G},3}(z+z_L-2z_{m+1})} \tag{12}$$

The above reflection coefficients for the x and y field components of the incident and radiated fields are related to the well-known reflection coefficients for a multi-layer dielectric parallel and perpendicular to the plane of incidence by:

$$R_{\bar{G}(1,2)\pm} = \frac{R_{\parallel,\perp}(k_1-G_1)^2 + R_{\perp,\parallel}(k_2-G_2)^2}{(k_1-G_1)^2+(k_2-G_2)^2} \tag{13a}$$

$$R_{\bar{G}\otimes\pm} = \frac{(R_{\parallel}-R_{\perp})(k_1-G_1)(k_2-G_2)}{(k_1-G_1)^2+(k_2-G_2)^2} \tag{13b}$$

Coefficients for the radiated fields $\Psi^a_{\bar{G}(1,2)+}$ and $\Psi^b_{\bar{G}(1,2)-}$ on either side of the array are related by using the boundary condition that the transverse electric field is continuous across the lattice.

$$\Psi^b_{\bar{G}(1,2)-} = \Pi_{\bar{G}(1,2)} \Psi^a_{\bar{G}(1,2)+} + \chi_{\bar{G}(2,1)} \Psi^a_{\bar{G}(2,1)+} \tag{14}$$

The dielectric internal reflection factors $\Pi_{\bar{G}(1,2)}$ and $\chi_{\bar{G}(2,1)}$ are for notational convenience and are defined below in Eq.s (15a-b).

$$\Pi_{\bar{G}(1,2)} = \frac{S_{\bar{G}(2,1)}(z_L) C_{\bar{G}(1,2)}(z_L) - R_{\bar{G}\otimes-} R_{\bar{G}\otimes+} e^{2i(\alpha_{\bar{G}m} - \alpha_{\bar{G}m+1})}}{S_{\bar{G}1}(z_L) S_{\bar{G}2}(z_L) - R^2_{\bar{G}\otimes-} e^{4i\alpha_{\bar{G}m}}} \tag{15a}$$

$$\chi_{\bar{G}(1,2)} = \frac{S_{\bar{G}(1,2)}(z_L) R_{\bar{G}\otimes+} e^{-2i\alpha_{\bar{G}m+1}} - C_{\bar{G}(1,2)}(z_L) R_{\bar{G}\otimes-} e^{2i\alpha_{\bar{G}m}}}{S_{\bar{G}1}(z_L) S_{\bar{G}2}(z_L) - R^2_{\bar{G}\otimes-} e^{4i\alpha_{\bar{G}m}}} \tag{15b}$$

The constant $\alpha_{\bar{G}m} = k_{\bar{G},3}(z_L - z_m)$ is the phase shift for a given mode away from the array. Equations (9), (11), and (14) allow the field radiated by the array to be expressed by a single pair of field amplitude coefficients , $\Psi^a_{\bar{G}1+}$ and $\Psi^a_{\bar{G}2+}$, in region "m" on either side of the array.

To derive a matrix equation for the radiated field amplitude coefficients, $\Psi^a_{\bar{G}1+}$ and $\Psi^a_{\bar{G}2+}$, the incident and radiated fields given by Eq.s (7), (9), (11), and (14) are substituted into Eq. (1). The resulting equation is then integrated term-by-term over z from $z_L-\Delta$ to $z_L+\Delta$, where Δ is a vanishingly small number. The nonvanishing terms due to the discontinuity at the array lead to an equation which can be solved to obtain the desired radiated field amplitude coefficients. The method is outlined below.

The integral of the first term in Eq. (1) is

$$\int_{z_L-\Delta}^{z_L+\Delta} \nabla^2 \mathrm{E}_{1,2} dz = \left.\frac{\partial \Psi^a_{1,2}(\vec{r})}{\partial z}\right|_{z_L+\Delta} - \left.\frac{\partial \Psi^b_{1,2}(\vec{r})}{\partial z}\right|_{z_L-\Delta} . \tag{16}$$

After some algebra, the integral is written in the form

$$\int_{z_L-\Delta}^{z_L+\Delta} \nabla^2 \mathrm{E}_{1,2} dz = i\sum_{\bar{G}} k_{\bar{G},3}\left(T_{\bar{G}(1,2)}\Psi^a_{\bar{G}(1,2)+} + T^{\otimes}_{\bar{G}(2,1)}\Psi^a_{\bar{G}(2,1)+}\right)e^{i(\vec{k}_T-\vec{G})\bullet\vec{r}} . \tag{17}$$

The dielectric reflection-based coefficients in Eq. (17) are defined as

$$T_{\bar{G}(1,2)} = (1-R_{\bar{G}(1,2)+}e^{-2i\alpha_{\bar{G}m+1}}) + \Pi_{\bar{G}(1,2)}(1-R_{\bar{G}(1,2)-}e^{2i\alpha_{\bar{G}m}}) - \chi_{\bar{G}(1,2)}R_{G\otimes-}e^{2i\alpha_{\bar{G}m}} \tag{18a}$$

$$T^{\otimes}_{\bar{G}(1,2)} = -R_{G\otimes+}e^{-2i\alpha_{\bar{G}m+1}} - \Pi_{\bar{G}(1,2)}R_{G\otimes-}e^{2i\alpha_{\bar{G}m}} + \chi_{\bar{G}(1,2)}(1-R_{\bar{G}(2,1)-}e^{2i\alpha_{\bar{G}m}}) . \tag{18b}$$

The second term of the wave equation is evaluated by consideration of Gauss's law, $\nabla \bullet \vec{E} = \rho/\varepsilon$, and the continuity equation, $\nabla \bullet \vec{J} = -\frac{\partial \rho}{\partial t}$. These lead to

$$\nabla \bullet \vec{E} = -\frac{i}{\omega\varepsilon}\left(\frac{\partial J_1}{\partial x} + \frac{\partial J_2}{\partial y}\right). \tag{19}$$

Current density components are related to the transverse field and surface resistivity by Eq. (2). Since the surface admittance of the array, $Y_s(x,y) \equiv 1/R_s(x,y)$, is a periodic function, it can be expanded as a sum of exponential basis functions.

$$Y_s(x,y) = \sum_{\vec{G}} Y_{\vec{G}} e^{-i\vec{G}\bullet\vec{r}} \tag{20}$$

Equation (2) is substituted into Eq. (19). Both surface admittance and the radiated field components are expressed as a sum of the exponential basis functions. The result, after integrating across the array over z, is

$$\int_{Z_L-\Delta}^{Z_L+\Delta}\left[\nabla(\nabla\bullet\vec{E})\right]_{1,2}dz=\frac{i}{\omega\varepsilon}\sum_{\vec{G}}\sum_{\vec{G}'}Y_{\vec{G}'}\{(k_{1,2}-G'_{1,2})[(\sum_{j=1}^{2}(k_j-G'_j)E_{j-}S_{0j}(z_L))$$
$$+((k_1-G'_1)E_{2-}+(k_2-G'_2)E_{1-})R_{0\otimes-}e^{2i\alpha_{0m}}]e^{-i\vec{G}'\bullet\vec{r}}$$
$$+(k_{1,2}-G_{1,2}-G'_{1,2})[(\sum_{j=1}^{2}(k_j-G_j-G'_j)\Psi^a_{\vec{G}j+}C_{\vec{G}j}(z_L)) \qquad (21)$$
$$+((k_1-G_1-G'_1)\Psi^a_{\vec{G}2+}+(k_2-G_2-G'_2)\Psi^a_{\vec{G}1+})R_{\vec{G}\otimes+}e^{-2i\alpha_{\vec{G}m+1}}]$$
$$e^{-i(\vec{G}+\vec{G}')\bullet\vec{r}}\}e^{i\vec{k}_T\bullet\vec{r}}$$

In a similar way, the integral of third term of the wave equation is found by substitution of Eq. (2).

$$i\omega\mu_0\int_{Z_L-\Delta}^{Z_L+\Delta}J_{1,2}dz=i\omega\mu_0\sum_{\vec{G}}\sum_{\vec{G}'}Y_{\vec{G}'}[(E_{1,2-}S_{0(1,2)}(z_L)+R_{0\otimes-}E_{2,1-}e^{2i\alpha_{0m}})e^{-i\vec{G}'\bullet\vec{r}} \qquad (22)$$
$$+(\Psi^a_{\vec{G}(1,2)+}C_{\vec{G}(1,2)}(z_L)+R_{\vec{G}\otimes+}\Psi^a_{\vec{G}(2,1)+}e^{-2i\alpha_{\vec{G}m+1}})e^{-i(\vec{G}+\vec{G}')\bullet\vec{r}}]e^{i\vec{k}_T\bullet\vec{r}}$$

Because the transverse components of the electric field are continuous across the array, the integral of the fourth term of the wave equation is zero.

The z-integrated wave equation is arrived at by adding Eq.s (17), (21), and (22) for the individual terms. Summations in the resulting equation are carried out over both $\vec{G}$ and $\vec{G}'$. To obtain a form which can be solved for the radiated field amplitudes, the resultant equation is first multiplied by $-ie^{i(\vec{G}''-\vec{k}_T')\bullet\vec{r}}$, then integrated over the x - y plane. The exponential basis functions are orthogonal, allowing for

one of the summations to vanish. A general equation for the radiated electric field amplitudes is found.

$$
\begin{aligned}
&(T_{\bar{G}(1,2)}\Psi^{a}_{\bar{G}(1,2)+}+T^{\otimes}_{\bar{G}(2,1)}\Psi^{a}_{\bar{G}(2,1)+})-\frac{1}{\omega\varepsilon k_{\bar{G},3}}\{(k_{1,2}-G_{1,2})[(\sum_{j=1}^{2}(k_j-G_j)E_{j-}S_{0j}(z_L))\\
&+((k_1-G_1)E_{2-}+(k_2-G_2)E_{1-})R_{0\otimes-}e^{2i\alpha_{0m}}]Y_{\bar{G}}\\
&+(k_{1,2}-G_{1,2})\sum_{\bar{G}'}[(\sum_{j=1}^{2}(k_j-G_j)\Psi^{a}_{\bar{G}'j+}C_{\bar{G}'j}(z_L))\\
&+((k_1-G_1)\Psi^{a}_{\bar{G}'2+}+(k_2-G_2)\Psi^{a}_{\bar{G}'1+})R_{\bar{G}'\otimes+}e^{-2i\alpha_{\bar{G}'m+1}}]Y_{\bar{G}-\bar{G}'}\}\\
&+\frac{\omega\mu_0}{k_{\bar{G},3}}[(E_{1,2-}S_{0(1,2)}(z_L)+R_{0\otimes-}E_{2,1-}e^{2i\alpha_{0m}})Y_{\bar{G}}\\
&+\sum_{\bar{G}'}(\Psi^{a}_{\bar{G}'(1,2)+}C_{\bar{G}'(1,2)}(z_L)+R_{\bar{G}'\otimes+}\Psi^{a}_{\bar{G}'(2,1)+}e^{-2i\alpha_{\bar{G}'m+1}})Y_{\bar{G}-\bar{G}'}]=0
\end{aligned}
\tag{23}
$$

This general equation can be put in a matrix form and solved. Considerable simplification is obtained, however, in cases where the coupling between the x and y components of the electric field can be neglected. Then the number of matrix elements is reduced by a factor of four, enabling much faster solutions.

For the remaining analysis, neglect the coupling between the x and y field components. Equations (15a-b) and Eq.s (18a-b) reduce to

$$
\begin{aligned}
&\Pi_{\bar{G}(1,2)}=\frac{C_{\bar{G}(1,2)}(z_L)}{S_{\bar{G}(1,2)}(z_L)}\\
&\chi_{\bar{G}(1,2)}=0
\end{aligned}
\tag{24}
$$

and

$$T_{\bar{G}(1,2)} = (1 - R_{\bar{G}(1,2)+} e^{-2i\alpha_{\bar{G}m+1}}) + \Pi_{\bar{G}(1,2)}(1 - R_{\bar{G}(1,2)-} e^{2i\alpha_{\bar{G}m}})$$
$$T^{\otimes}_{\bar{G}(1,2)} = 0 \qquad (25)$$

Equation (23) simplifies to

$$T_{\bar{G}(1,2)} \Psi^{a}_{\bar{G}(1,2)+} - \frac{1}{\omega\varepsilon k_{\bar{G},3}}[(k_{1,2} - G_{1,2})^2 E_{1,2-} S_{0(1,2)}(z_L) Y_{\bar{G}}$$
$$+(k_{1,2} - G_{1,2})^2 \sum_{\bar{G}'} \Psi^{a}_{\bar{G}'(1,2)+} C_{\bar{G}'(1,2)}(z_L) Y_{\bar{G}-\bar{G}'}] \qquad (26)$$
$$+\frac{\omega\mu_0}{k_{\bar{G},3}}[E_{1,2-} S_{0(1,2)}(z_L) Y_{\bar{G}} + \sum_{\bar{G}'} \Psi^{a}_{\bar{G}'(1,2)+} C_{\bar{G}'(1,2)}(z_L) Y_{\bar{G}-\bar{G}'}] = 0$$

Equation (26) represents a set of $2N$ equations, where N is the product of the number of x and y reciprocal lattice vectors. Their solution yields the modes $\psi^{a}_{\bar{G}1+}$ and $\psi^{a}_{\bar{G}2+}$ which comprise the x and y components of the radiated electric field. An examination of Eq. (26) shows how each mode is coupled to the other modes through a capacitive term, proportional to $\frac{1}{\omega\varepsilon k_{\bar{G},3}}$, and an inductive term, proportional to $\frac{\omega\mu_0}{k_{\bar{G},3}}$. The equation shows how the amplitude of a particular mode is affected by parameters such as dielectric reflections, incident wave direction, and pattern shape. For numerical solution, Eq. (26) is written in the form of a matrix equation.

$$\left(\omega^2\overline{\overline{\mathbf{A}}}+\omega\overline{\overline{\mathbf{B}}}+\overline{\overline{\mathbf{C}}}\right)\bullet\overline{\mathbf{X}}=\omega^2\overline{\mathbf{D}}+\overline{\mathbf{F}}\,. \tag{27}$$

For either the x or y field components, elements of the square matrices $\overline{\overline{\mathbf{A}}}$, $\overline{\overline{\mathbf{B}}}$, and $\overline{\overline{\mathbf{C}}}$ are identified as

$$\begin{aligned}
A_{\bar{G},\bar{G}'} &= \frac{\mu_0}{k_{\bar{G},3}} C_{\bar{G}',i} Y_{\bar{G}-\bar{G}'} \\
B_{\bar{G},\bar{G}'} &= T_{Gi}\delta_{\bar{G},\bar{G}'} \\
C_{\bar{G},\bar{G}'} &= -\frac{1}{\varepsilon k_{\bar{G},3}}(k_i - G_i)^2 C_{\bar{G}',i} Y_{\bar{G}-\bar{G}'}
\end{aligned} \tag{28}$$

Elements of the column matrices $\overline{\mathbf{D}}$, $\overline{\mathbf{F}}$, and $\overline{\mathbf{X}}$ are

$$\begin{aligned}
D_{\bar{G}} &= -\frac{\mu_0}{k_{\bar{G},3}} E_{i-} S_{0,i}(z_L) Y_{\bar{G}} \\
F_{\bar{G}} &= \frac{1}{\varepsilon k_{\bar{G},3}}(k_i - G_i)^2 E_{i-} S_{0,i}(z_L) Y_{\bar{G}}\,. \\
X_{\bar{G}} &= \Psi^a_{\bar{G},i+}
\end{aligned} \tag{29}$$

Equation (29) can be solved using standard matrix inversion techniques. The column matrix $\overline{\mathbf{X}}$ contains the amplitude coefficients for the electric field Floquet modes radiated by the conducting array. These modes are plane waves. They are linked together by the coefficients for the array conductivity, $Y_{\bar{G}-\bar{G}'}$. Together with the incident field added in phase, and including the reflections at dielectric

boundaries, reflection and transmission coefficients are calculated in a straightforward manner.

III. EXPERIMENTAL VALIDATION

Accuracy of the theoretical analysis has been verified by a series of experimental measurements. Transmission measurements for a number of test devices exhibit a variety of striking characteristics, including resonances, which are well reproduced by calculations.

Results of experimental validation studies are presented for four test panels. For three panels the patterns were highly conductive. Correspondingly, the surface resistivity entered in the computations was chosen small enough to have no significant effect on the output. The test panels are approximately square with a length of 30 cm on each side. Measurements were performed in a transmission tunnel which contains two antennas for transmission and reception of microwave radiation inside a box lined with absorber material. A baffle following the transmitting antenna collimates the incident wave. Figure 2 displays a schematic of the experimental arrangement. Incident energy is normal to the array panel with the electric field polarized in the x direction, parallel with one edge of the square patterns. Measurements were made using a Hewlett Packard 8510C network

analyzer. Effects of spurious reflections, such as those off the wall, were minimized by suitably gating the signal in the time domain.

The first panel was fabricated from a commercial photosensitive printed circuit board. After etching, a pattern of thin copper squares remained on the 0.145 cm thick dielectric backing. The periodicity of the pattern is 1.0 cm in each direction and the copper square size is 0.9 cm. Electric permittivity (normalized to free space) of the dielectric was measured and found to have a real part of 4.4 and an imaginary part less than 0.1. Transmission was measured with the copper square pattern facing the incident wave. Matrix calculations included 129 modes in the direction of the incident field and 17 modes perpendicular to it (2193 unknowns). Resulting curves for both experiment and computation are shown in Fig. 3. As expected, the test panel acts as a low pass filter, with transmission decreasing with increasing frequency. Calculated and measured transmission differ by at most 0.05 over the entire frequency range. The frequency at which the wavelength of a plane wave propagating in the dielectric, λ_D, is equal to the array period, d_x, is noted on the graph. This is the frequency above which the lowest order secondary modes, $(n_1,n_2) = (\pm 1,0)$ and $(0,\pm 1)$, can propagate in the dielectric, as can be seen from Eq. (6). Physically, the array constrains these modes to have a periodicity which is a multiple of d_x in the x direction,

implying the x component of the propagation vector is $2\pi/d_x$. The vector sum of the x component and the z component (must be real) of the propagation vector must have a magnitude of $2\pi/\lambda_D$. This only is possible if $\lambda_D < d_x$. In the literature, these secondary modes are known as a grating lobes. Because of the total internal reflection by the dielectric slab, the grating lobes are trapped inside the dielectric until the frequency is above the point at which the free space wavelength, λ_{FS}, is less than d_x. The $(\pm 1, 0)$ and $(0, \pm 1)$ grating lobes then propagate away from the panel in a nonspecular direction. In general, higher order modes propagate when $k_{\bar{G},3}$, as given by Eq. (6), is real in the medium of interest.

A second test sample consists of an array of aluminum foil squares with a periodicity of 2.0 cm in each direction. The array is taped to a 0.01 cm thick paper backing. Total dielectric thickness, tape plus paper, is approximately 0.02 cm. Lengths of the squares' edges are 1.5 cm. For computations, the small effect of the paper backing was included by using a real permittivity of 5.1, found by earlier measurements. The tape was neglected. Calculations included 65 modes in the direction of the incident field and 17 modes perpendicular to it. Calculated and measured values of transmission are graphed in Fig. 4 (solid lines and circles). The panel is a low pass filter below the resonant

frequency, ω = 9.0×10^{10} rad/s. The primary mode, (0,0), is the only propagating mode up to this frequency. At resonance, the amplitude of the primary radiated mode peaks with an amplitude and phase which nearly cancel the incident wave. An examination of the field modes has shown that is due to the coupling of the incident field to the evanescent fields which has a 90° phase shift at this frequency. A second 90° phase shift occurs in the coupling from the evanescent fields to the radiated field, resulting in the net 180° phase difference between the incident and radiated primary field. A substantial loss in transmission results, which is clear in the figure. For a given periodicity, we observed that the resonant frequency is dependent on pattern dimensions. The resonant behavior can be modeled as a circuit analog. Figure 4 (dashed lines and x's) also shows the results of measurements and calculations for the same geometry, but with the conductive patterns cut from a sheet having a surface resistivity of 53 $\Omega_{\square}$. As expected from circuit considerations, the resistivity dampens the resonant peak, but otherwise the shape of the curves are similar. Above ω = 9.4×10^{10} rad/s, $\lambda_{FS} < d_x$ and the modes (±1,0) and (0,±1) begin to propagate away from the panel. This follows from the arguments given in the previous paragraph. These modes propagate in a nonspecular direction with a polar angle given by $\cos\theta = k_{\vec{G},3} / \beta_0$ and therefore to not contribute directly to the transmission coefficient. The excellent agreement with

measured data is also evident in Fig. 4. Resonances in the transmission spectrum have historically been referred to as Wood's anomalies, which were associated with the onset of propagation of grating lobes in slot arrays for the free space case [12]. The resonances here are analogous.

The fourth panel consists of an a array on 1.5 cm aluminum squares with a 2.0 cm periodicity like in the previous figure. In this case, it is backed by a 0.54 cm thick Plexiglas sheet. Calculations included 65 modes in the direction of the incident field and 17 modes perpendicular to it. Calculated and measured results are compared in Fig. 5. The addition of a dielectric backing has resulted in two resonance peaks, one at 7.0×10^{10} and the other at 8.8×10^{10} rad/s. The $(\pm 1, 0)$ and $(0, \pm 1)$ modes are trapped by the dielectric in the frequency range from 6.2×10^{10} ($\lambda_D = d_x$) to 9.4×10^{10} rad/s ($\lambda_{FS} = d_x$). Above 8.8×10^{10} rad/s, $\lambda_D = \frac{1}{\sqrt{2}} d_x$ and the $(\pm 1, \pm 1)$ modes can propagate in the dielectric, but not in free space. These frequency intervals are indicated in the figure. Agreement is quite good between the measured and calculated results. Observed discrepancies have a number of possible causes. Calculations assume the planar array is infinite in extent. Yet, the baffle which limits the beam size is 20 cm in diameter, equivalent to 10 array periods for this panel. Departures of the incident beam wave front from the assumed plane wave can also be significant.

IV. CONCLUSION

A new method for analyzing the electric field scattered by a planar periodic array of conductive elements in a stratified dielectric has been developed. The analogy of these structures with photonic devices was exploited in formulating the technique. Coupling between radiated field modes as well as with the incident field is given by a single equation which can be solved by matrix inversion techniques. Since mode coupling determines overall performance, this approach may lead to better understanding of scattering by these structures. Periodically varying conducting elements are expressed as a sum of exponential basis functions, allowing for arbitrarily shaped complex impedance distributions with a continuous or discontinuous profile to be used. This enables increased design flexibility.

Theoretical predictions were made for a variety of configurations, from a computer program based upon this method. Accuracy of the method was demonstrated by comparing experimental transmission measurements with the model's predictions. Results were in excellent agreement with calculations. Frequencies at which grating lobes appear were noted. This method can be extended to multilayered periodic

structures, using the generalized scattering matrix approach, in a straightforward manner.

ACKNOWLEDGMENT

The author acknowledges the encouragement for suggesting the problem and editorial review by Dr. Donald Forester. Several insightful discussions were provided by Mr. Elee Dumas, Dr. John Schelleng, and Dr. Douglas Taylor. The experimental validation assistance by Mr. Scott Browning, Mr. Jonas Lodge, Dr. Douglas Smith, and Mr. David Smith is greatly appreciated.

FOOTNOTE

This work was supported in part by the Office of Naval Research basic research program, NRL core program. It was also supported in part by a grant of HPC time from the DOD HPC center, NRL SGI Power Challenge computer.

The author is with the Naval Research Laboratory, Washington, D. C. 20375.

REFERENCES

1. T. K. WU, "Fundamentals of Periodic Structures," in *Frequency Selective Surface and Grid Array*, ch. 1, T. K. Wu and K. Chang, Eds. New York: Wiley, 1995.
2. R. Mittra, C. H. Chan, and T. Cwik, "Techniques for Analyzing Frequency Selective Surfaces-A Review," in *Proc. IEEE*, Dec. 1988, vol. 76, pp. 1593-1615.
3. C. H. Chan, "Analysis of Frequency Selective Surfaces," in *Frequency Selective Surface and Grid Array*, ch. 2, T. K. Wu and K. Chang, Eds. New York: Wiley, 1995.
4. C. Wan and J. A. Encinar, "Efficient Computation of Generalized Scattering Matrix for Analyzing Multilayered Periodic Structures," *IEEE Trans. Antennas Propagat.*, vol. 43, pp. 1233-1242, Nov. 1995.
5. R. C. Hall, R. Mittra, and K. M. Mitzner, "Analysis of Multilayered Periodic Structures Using Generalized Scattering Matrix Theory," *IEEE Trans. Antennas Propagat.*, vol. 36, pp. 511-517, April 1988.
6. J. M. Usoff, "Electromagnetic Scattering from Infinite Periodic Arrays of Rectangular Elements of Arbitrary Permittivity and Permeability in a General Stratified Medium," Master's thesis, Ohio State Univ., Columbus, OH; 1886.
7. B. A. Munk, "A General Theory of Periodic Surfaces in a Stratified Dielectric Medium," Tech. Report 715582-4,

ElectroScience Lab., Ohio State Univ., Columbus, OH, Feb. 1986.

8. T. K. WU, "Multiband Frequency Selective Surfaces," in *Frequency Selective Surface and Grid Array*, ch. 4, T. K. Wu and K. Chang, Eds. New York: Wiley, 1995.

9. F. Stefan Johansson, L. Robert Lagerholm, and Per-Simon Kildal, "Frequency-Scanned Reflection Gratings with Integrated Polarizer," *IEEE Trans. Antennas Propagat.*, vol. 40, pp. 331-334, March 1992.

10. D. R. Smith, R. Dalichaouch, N. Kroll, S. Schultz, S. L. McCall, and P. M. Platzman, "Photonic Band Structure, and Defects in One and Two Dimensions," *J. Opt. Soc. Am. B*, vol. 10, pp. 314-321, Feb. 1993.

11. John Sajeev, "The Localization of Light", in Photonic Band Gaps and Localiztion, pp. 1-22, C. M. Soukoulis, Ed. New York, Plenum Press, 1993.

12. R. J. Luebbers and B. A. Munk, "Some Effects of Dielectric Loading on Periodic Slot Arrays," *IEEE Trans. Antennas Propagat.*, vol. 26, pp. 536-542, July 1978.

FIGURE CAPTIONS

1. (a) Thin, conducting array in the x - y plane with periodicity d_x and d_y. (b) The planar array at $z = z_L$ imbedded in a multilayered dielectric medium (z_1 to z_M).
2. Experimental configuration used to measure the transmission coefficients.
3. Comparison of calculated with measured values of transmission through an array of copper squares having a 1.0 cm periodicity backed by a 0.145 cm thick dielectric sheet.
4. Comparison of measured and calculated transmission for two different square arrays (aluminum and and 53 $\Omega_{\square}$), each with a 2.0 cm periodicity. Calculated and measured values for the periodic Al array are represented by solid lines and open circles. The resonant dip at 90×10^9 rad/s is due to the coupling between the incident and evanescent fields which are 90^0 out of phase at this point. For the periodic resistive array, calculated and measured transmission are represented by dashed lines and x's.
5. Comparison of calculated and measured transmission through an array of aluminum squares having a 2.0 cm periodicity. The array is backed by a Plexiglas sheet having a thickness of 0.54 cm.

Figure 1

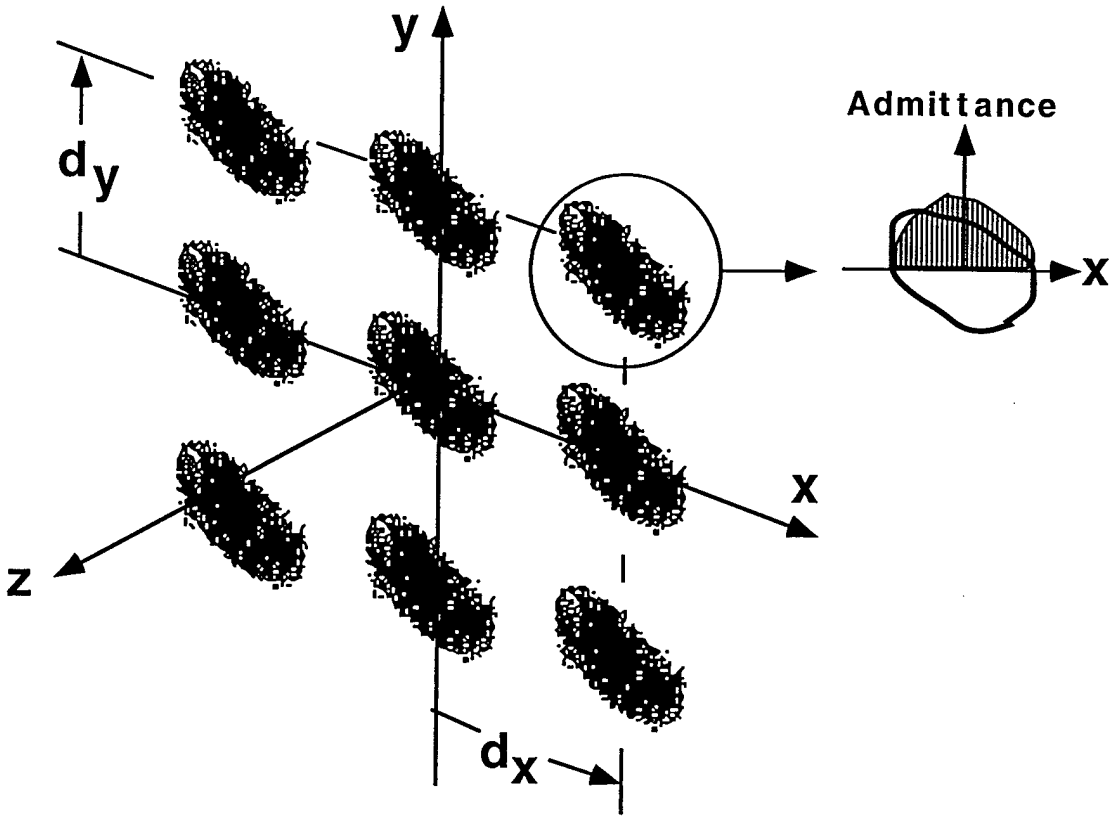
y
Admittance
d_y
x
x
z
d_x

(a)

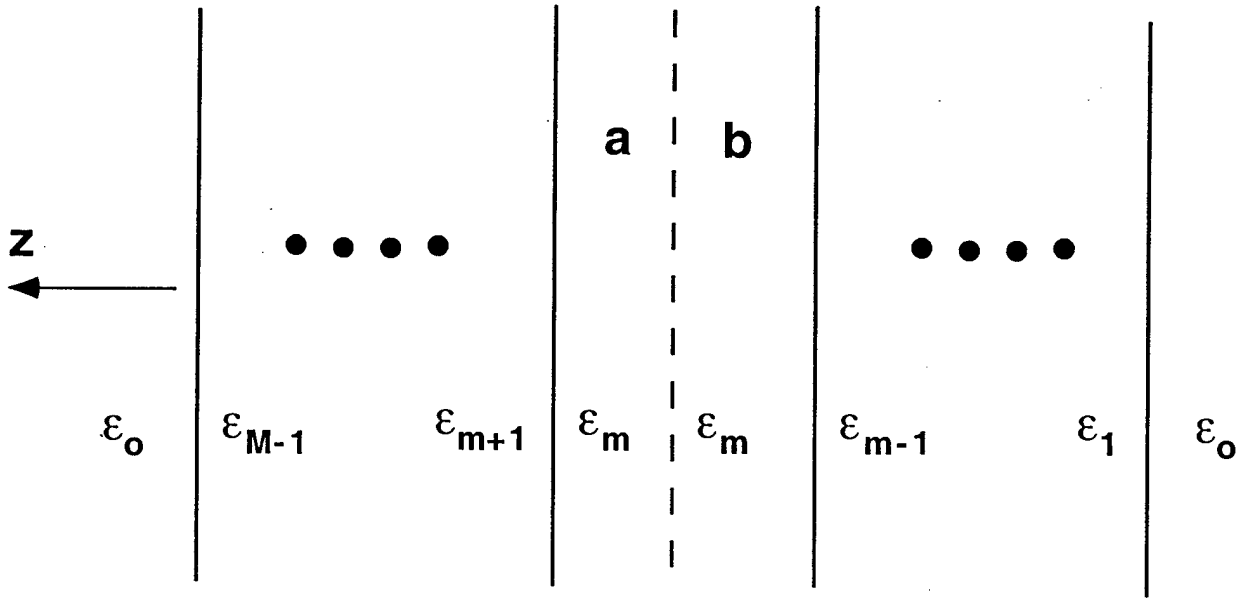
a
b
z
ε_o
ε_{M-1}
ε_{m+1}
ε_m
ε_m
ε_{m-1}
ε_1
ε_o
z_M
z_{m+1}
z_L
z_m
z_1

(b)

Figure 2

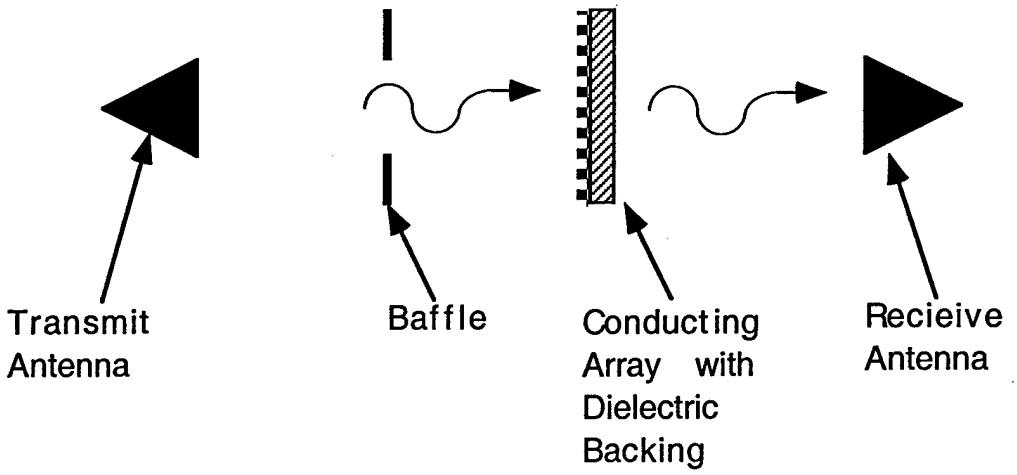
Transmit
Antenna
Baffle
Conducting
Array with
Dielectric
Backing
Recieive
Antenna

Figure 3

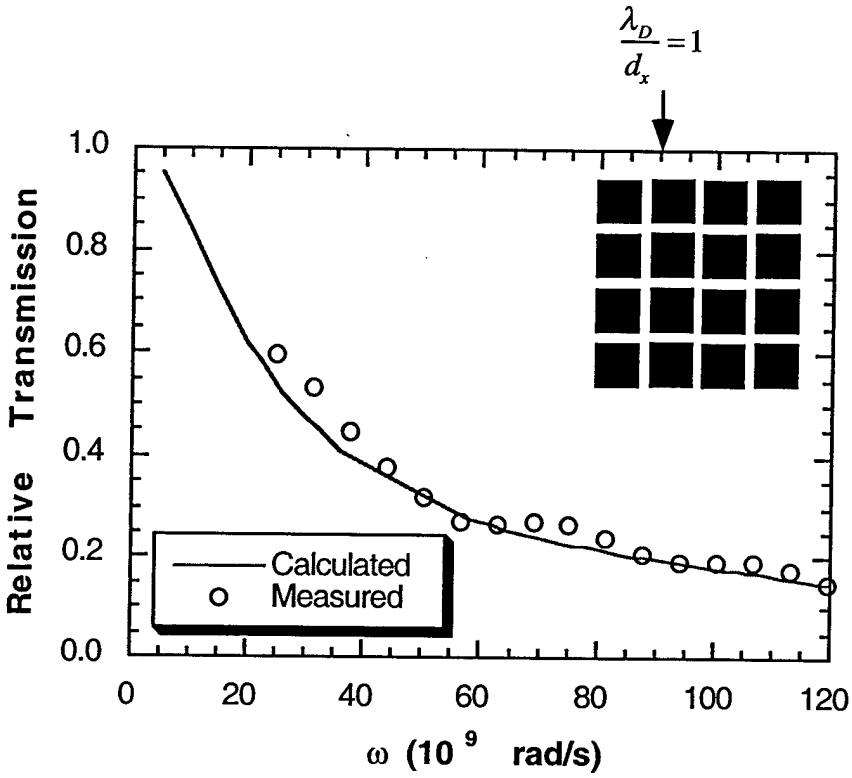
$\frac{\lambda_D}{d_x} = 1$
Relative Transmission
1.0
0.8
0.6
0.4
0.2
0.0
0
20
40
60
80
100
120
ω (10 9 rad/s)
Calculated
Measured

Figure 4

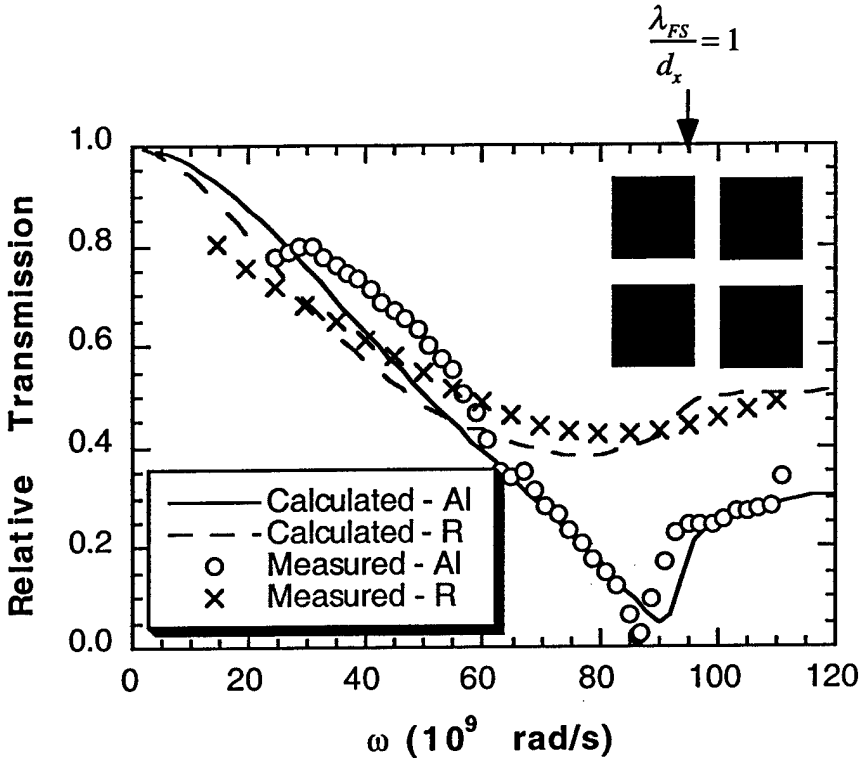
$\frac{\lambda_{FS}}{d_x} = 1$
1.0
0.8
0.6
0.4
0.2
0.0
Relative Transmission
0
20
40
60
80
100
120
ω (10^9 rad/s)
Calculated - Al
Calculated - R
Measured - Al
Measured - R

Figure 5

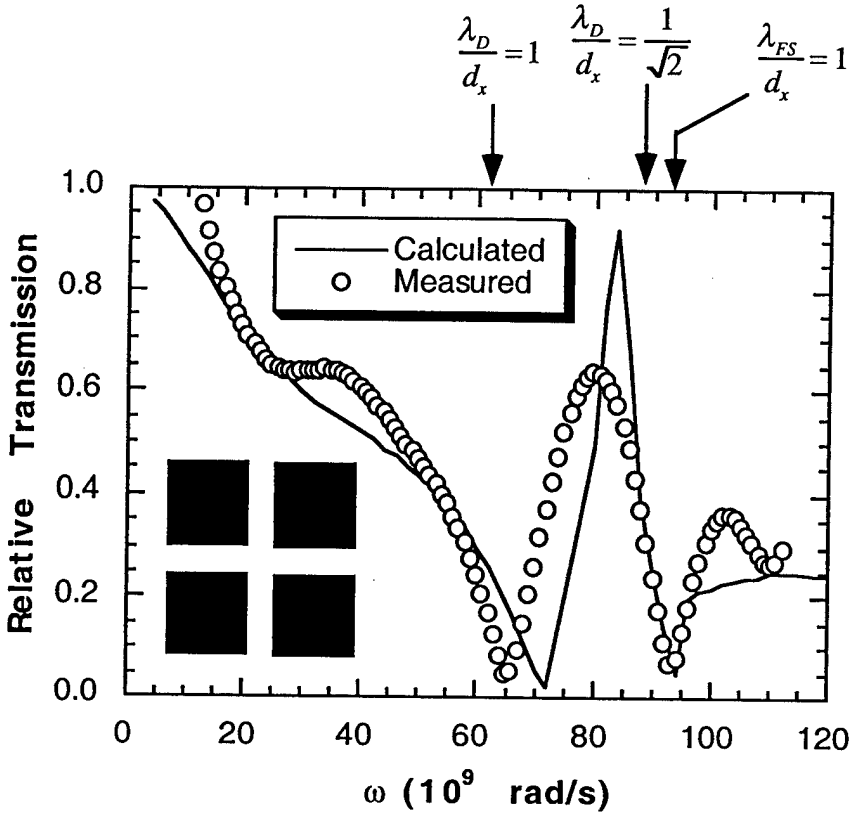
$\frac{\lambda_D}{d_x}=1$
$\frac{\lambda_D}{d_x}=\frac{1}{\sqrt{2}}$
$\frac{\lambda_{FS}}{d_x}=1$
Calculated
Measured
Relative Transmission
1.0
0.8
0.6
0.4
0.2
0.0
0
20
40
60
80
100
120
ω (10^9 rad/s)